J Solid State Electrochem (2006) 10: 469–478
DOI 10.1007/s10008-005-0020-z

ORIGINAL PAPER

Alain Walcarius

Zeolite-modified paraffin-impregnated graphite electrode

Received: 27 March 2005 / Revised: 12 April 2005 / Accepted: 20 May 2005 / Published online: 27 July 2005

Abstract This paper describes a new kind of zeolite-modified electrodes (ZMEs) based on the physical immobilization of zeolite particles onto the surface of paraffin-impregnated graphite electrodes (PIGEs). Their electrochemical behavior was first evaluated by ion-exchange voltammetry using methylviologen as a model redox probe, indicating better performance in comparison to the corresponding zeolite-modified carbon paste electrodes. The zeolite-modified-PIGEs were then applied to the study of lead(II)-loaded zeolites to monitor their reaction with sulfide ions at various sulfidation levels. Both Pb(II) ions and PbS nanoparticles gave rise to well-defined voltammetric signals, but peak currents due to the more mobile Pb(II) ions were much higher than those recorded for PbS nanoparticles. This is due to the fact that Pb(II) ions underwent ion exchange for the electrolyte cation prior to the electron transfer whereas the PbS nanoparticles are immobilized in the microporous structure of the zeolite particles and thus less available for the redox reactions. Nevertheless, these signals were useful to discriminate between the various sulfidation levels, as ascertained by additional X-ray photoelectron spectroscopy measurements.

Keywords Zeolite-modified electrode · PIGE · Ion exchange · Lead · PbS · Voltammetry

Introduction

Zeolite-modified electrodes (ZMEs) have been largely developed during the past two decades because they enable to combine the intrinsic properties of the crystalline aluminosilicates (mainly their ion-exchange capacity and their size selectivity at the molecular level) with electron transfer reactions [1]. This has led to numerous applications, including electrocatalysis, voltammetric detection based on preconcentration and/or permselectivity, indirect amperometric detection, potentiometric sensing, electrochemical biosensors, solid electrolytes, and photoelectrochemistry, as reported in several well-documented reviews or monographs [1–7].

Due to their electronically insulating character, however, zeolite particles must be arranged in close contact to an electrode material to be exploited for electrochemical purposes. This is not an easy task so that various strategies have been proposed in the literature:

1) Zeolite/polymer (with or without carbon) coatings deposited on solid electrode surfaces (see, e.g., [8–14]);
2) Zeolite particles dispersed in conductive carbon-based composite matrices (see, e.g., [14–19]);
3) Pressed zeolite + carbon mixtures or pellets made of pressed zeolite powder (see, e.g., [20–25]);
4) Zeolite/polymer membranes (see, e.g., [26–28]);
5) Zeolite dispersion and slurries between two feeder electrodes (see, e.g., [7, 29, 30]);
6) Continuous zeolite films synthesized on solid electrodes (see, e.g., [31–34]).

Zeolite overlayers on electrode surfaces constitute an attractive approach but they may suffer from rather poor mechanical stability, which required most often the use of an organic polymer (as a binder in mixture with zeolite particles [8–10], or deposited onto zeolite monograin- or multi-layers [11, 12]) to prevent zeolite particles from leaching in the solution. Zeolite-modified carbon paste electrodes have been largely and successfully applied for electroanalytical purposes [1, 4, 6], but they are characterized by significant ingress of the electrolyte and/or analyte solution inside the composite matrix (as a consequence of the hydrophilic character of the zeolite)

A. Walcarius
Laboratoire de Chimie Physique et Microbiologie pour l'Environnement,Unité Mixte de Recherche UMR 7564, CNRS—Université H. Poincaré Nancy I, 405, rue de Vandoeuvre, 54600 Villers-les-Nancy, France
E-mail: walcarius@lcpme.cnrs-nancy.fr
Tel.: +33-383-685259
Fax: +33-383-275444

during the electrochemical experiments [35, 36], leading to undesired memory effects that might be mostly solved by the resort to zeolite-modified "solid" carbon paste electrodes [37].

In this work, a new kind of ZME is introduced involving zeolite particles mechanically immobilized on paraffin-impregnated graphite rod electrodes (PIGEs). This has been achieved by exploiting the abrasive transfer techniques, otherwise developed for the electrochemical analysis of solid electroactive compounds [38]. Actually, the application of this technique to non-redox solids (but likely to interact with redox active species) is not widespread [39], and it can be anticipated that this approach would be promising in the field of ZMEs in view of effective immobilization of zeolite particles on the electrode surface in a configuration avoiding any impregnation of the bulk electrode by the surrounding solution. This will be illustrated here in the case of the ion exchange voltammetry of methylviologen at zeolite-modified PIGEs. The novel kind of ZME will be also used to study lead-loaded zeolite particles and to monitor their sulfidation. This second example will give the opportunity to compare the electrochemical response of ZMEs exhibited with ion-exchanged and thus mobile species (Pb^{2+}) to that observed for confined, yet conductive, clusters (PbS) in/on the insulating zeolite particles. Lead(II) species are indeed known to accommodate the ion-exchanging sites in many zeolites [40–42], which was notably exploited for remediation purposes, [43–45], but the electrochemistry of lead-loaded zeolites was only sparingly considered [32, 46]. On the other hand, no data are available on the electrochemical behavior of lead sulfide moieties supported on/within zeolite molecular sieves.

Experimental

Chemicals and reagents

All chemicals and reagents were analytical grade, and solutions were prepared with high purity water (18 MΩ cm) from a Millipore Milli-Q water purification system. Methylviologen (N,N′-dimethyl-4,4′-bipyridinium dichloride, $MVCl_2$) was purchased from Aldrich while $Pb(NO_3)_2$, Na_2S, NaOH, acetic acid, citric acid, and $NaNO_3$ were obtained from Prolabo.

Zeolite samples and electrode preparation

Zeolite Y was the Linde Molecular Sieve Cat. Base L-Y54 powder (sodium form; average particle size: 0.5–2 μm; chemical composition: $Na_{56}Al_{56}Si_{136}O_{384}{\cdot}250H_2O$; ion-exchange capacity: 3.4 meq g^{-1}; pore aperture: 8.1 Å) obtained from UOP, Molecular Sieve Division. Zeolite A was Linde 4A (sodium form; average particle size: 3–5 μm chemical composition: $Na_{12}Al_{12}Si_{12}O_{48}{\cdot}27H_2O$; ion-exchange capacity: 5.6 meq g^{-1}; pore aperture: 3.9 Å) supplied by Aldrich. These zeolites in their sodium form have been denoted NaY and NaA, respectively.

The methylviologen (MV^{2+}) and Pb(II) forms of zeolite Y were typically obtained by allowing to react 1 g of the powdered solid suspended in a 100 mL of an aqueous solution containing either 0.10 M $MVCl_2$ or 0.012 M $Pb(NO_3)_2$, under constant stirring for 48 h. The zeolite particles were then filtered and washed several times with high purity water and allowed to dry in air. The experimental exchange capacity was determined by ICP-AES (Plasma 2000, Perkin Elmer) for Pb(II) and by spectrophotometry for MV^{2+} [47], after decomposition of the zeolite framework with citric acid (0.10 g ion-exchanged zeolites in 5.00 mL aqueous 0.1 M citric acid solution) leading to the leaching of exchanged ions into the solution [8]. The ion-exchanged samples of zeolite Y used in this work contained respectively 1.1 mmol g^{-1} of Pb(II) species and 1.0 mmol g^{-1} of MV^{2+}. Even if incompletely exchanged zeolites were used (some remaining Na^+ counterions), they have been denoted PbY and MVY, respectively, afterwards.

Sulfidation of lead-loaded zeolites was performed by suspending typically 1 g of PbY particles in 100 mL solution containing various Na_2S concentrations ranging from $5{\times}10^{-4}$ M to $1.5{\times}10^{-2}$ M. The reaction was very fast (completed within 5 min) and the initially white zeolite particles became instantaneously dark/black once contacting the sulfide medium. The particles were collected by filtration and allowed to dry in an oxygen-free atmosphere, while the supernatant was discarded and kept for further analyses of consumed S^{2-} and Na^+ species (to evaluate the yield of the sulfidation reaction and charge balance in the zeolite).

The paraffin-impregnated graphite electrode (PIGE) was prepared as previously described [38], by impregnating spectroscopic graphite rods (3 mm in diameter) with a melted paraffin wax (m.p. 58–60 °C, from Fluka) under reduced pressure. Its surface was polished mechanically on a filter paper. The powdered zeolites were transferred and immobilized onto the electrode surface by the abrasive transfer technique [38]. This was typically achieved by placing some micrograms of the zeolite sample on a clean glazed porcelain tile to form a spot of finely distributed particles and gently rubbing the lower circular surface of the PIGE on this spot to transfer the sample to the electrode surface. The PIGE was then gently scrubbed on a glass substrate to remove ill-adhered particles.

Instrumentation

Cyclic voltammetry (CV) experiments were carried out using the Model 263 potentiostat (EG &G Princeton Applied Research) and the current versus potential curves were plotted with the aid of an X-Y recorder (Kipp & Zonen). For presentation, the CV curves obtained for lead-doped zeolites and lead sulfide species have been digitalized with the CurveUnscan software,

while the (multisweep) cyclic voltammograms recorded for methylviologen are presented as scanned pictures (because of too numerous curves). The measurements were performed at 25 °C with a three-electrode system mounted on a 50-mL cell containing the supporting electrolyte (0.1 M $NaNO_3$) at a concentration of 0.1 M. The counter-electrode was a platinum wire and a calomel electrode (Radiometer, N° XR 110) served as reference. Working electrodes were the homemade zeolite-modified paraffin-impregnated electrodes described above. Some zeolite-modified carbon paste electrodes were used for comparison purposes.

X-ray photoelectron spectroscopy (XPS) was used to monitor the sulfidation of PbY zeolites. The spectra were obtained using an electron energy analyzer (VSW, MCD 5000) and an unmonochromatized MgKα source (1253.6 eV). Powders were pressed onto the adhesive side of a copper adhesive electrical tape. The binding energies were corrected on the basis of the standard value of C_{1S} from contaminants at 284.6 eV. Narrow scanned spectra were used to obtain the chemical state information for lead.

Results and discussion

Ion-exchange voltammetry of MV^{2+}

Methylviologen (MV^{2+}) was first used as a model redox probe to evaluate the electrochemical behavior of the zeolite-modified PIGE. As shown in Fig. 1a, the presence of zeolite Y particles on the electrode surface lead to the progressive concentration of the positively-charged MV^{2+} species at the electrode/solution interface as successive potential cycling gave rise to an increase of peak currents, which were significantly higher than the CV response of the unmodified PIGE (compare curves "a" and "b" in Fig. 1a). This is clearly due to the accumulation of MV^{2+} in zeolite Y by ion exchange, in agreement to what has been previously reported for other kinds of ZMEs [8, 14, 35, 48, 49]. By contrast, no accumulation was observed when using the small pore zeolite A instead of the large pore zeolite Y because MV^{2+} ions are excluded from zeolite A due to steric effect (this zeolite can only accommodate cations of less than 4 Å in

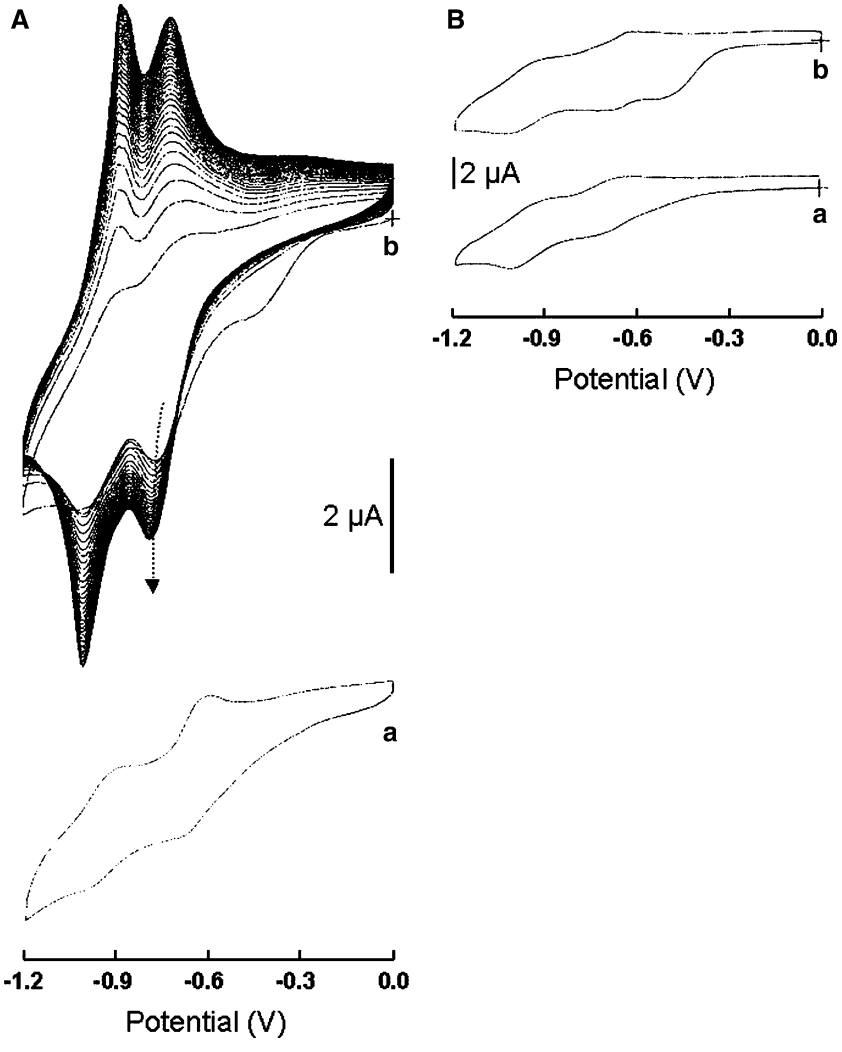

Fig. 1 Cyclic voltammograms recorded in 2×10^{-4} M MV^{2+} using unmodified PIGEs (curves "a" in **A**, **B**) and PIGEs modified with either NaY (curve "b" in **A**) or NaA (curve "b" in **B**) zeolite particles. The first 40 CV scans are depicted for the zeolite-Y- modified electrode (curve "b") in **A**) whereas only one cycle is shown for the unmodified and NaA-PIGEs as no effect of multiple potential scanning was observed in these cases. CV curves were recorded at scan rates of 10 mV s^{-1} (**A**) or 20 mV s^{-1} (**B**)

size, which is incompatible with the dimensions of MV^{2+} : 6.3×13.4 Å in its planar configuration [50])

Consistent with the extrazeolite electron transfer mechanism demonstrated for MV^{2+} in zeolite Y (i.e., MV^{2+} exchange for the supporting electrolyte cation (Eq. 1) prior to its electrochemical transformation (Eq. 2 a, b, c) [49, 51, 52]), the electrochemical behavior of these accumulated species is nearly identical to that of MV^{2+} in solution [53].

$$MV^{2+}_{(Z)} + 2C^{+}_{(S)} \rightleftharpoons MV^{2+}_{(S)} + 2C^{+}_{(Z)} \quad (1)$$

$$MV^{2+}_{(S)} + e^{-} \rightleftharpoons MV^{\bullet+}_{(S)} \quad (2a)$$

$$MV^{\bullet+}_{(S)} + e^{-} \rightleftharpoons MV^{0} \quad (2b)$$

$$MV^{2+} + MV^{0} \rightleftharpoons 2MV^{\bullet+} \quad (2c)$$

where subscripts S and Z refer to solution and zeolite, respectively, and C^{+} is the electrolyte cation.

Note that even this extrazeolite mechanism is the dominant process responsible for the electron transfer reactions of MV^{2+} exchanged in zeolite Y [8, 49, 51, 52], the existence of possible intervention of intrazeolite electron transfer was also mentioned in the literature [54]. MV^{2+} electrochemistry is characterized by two successive one-electron transfers corresponding to the reduction of the divalent cation MV^{2+} into the corresponding cation-radical $MV^{\bullet}$ (at −0.7 V, Eq. 2a), which is then reduced into the neutral species MV^{0} (at −1.0 V, Eq. 2b), this last electron transfer reaction being somewhat less reversible than the first one because of the possible existence of comproportionation of the final neutral product with the parent MV^{2+} (Eq. 2c). The pre-wave appearing at about −0.4 V is due to the reduction of residual oxygen catalyzed by methylviologen [16, 55, 56], which was much more pronounced for the zeolite-modified PIGEs (curves "b" in Fig. 1) that for the unmodified electrodes (curves "a" in Fig. 1) because of the presence of trapped oxygen in zeolite particles [57]. Finally, one has to note that the oxidation of zerovalent MV^{0} occurred here in the form of a single peak (located at −0.88 V), which is indicative of a single phase MV^{0} deposit on the PIGE surface, contrarily to what was observed with zeolite monograin layers on glassy carbon electrodes for which amorphous and crystalline MV^{0} deposits can be distinguished via two separate anodic signals [52]. At this stage, one cannot observe significant differences between the properties of zeolite-modified PIGEs and, e.g., zeolite-modified carbon paste electrodes [18, 50].

Figure 2a depicts the multisweep cyclic voltammograms recorded in a MV^{2+}-free electrolyte solution using a zeolite-modified PIGE that was prepared from MV^{2+}-loaded zeolite particles (MVY with 1.0 mmol g^{-1} of MV^{2+}). In this case, contrary to the data of Fig. 1, the electrochemical response of the electrode is entirely due to MV^{2+} species originating from the zeolite particles and not from the solution. As shown (Fig. 2a), the intensity of the voltammetric signals dropped dramatically once scanning potentials, leading to peak currents for the tenth cycle of less than 10% relative to those of the first scan. This decrease is explained by the continuous leaching of MV^{2+} species from the zeolite particles by ion-exchange for the electrolyte cation (associated or not to the electron transfer processes, Eqs. 1, 2). Moreover, it was much more pronounced with the MVY-modified PIGE than with a carbon paste electrode modified with the same MVY zeolite particles for which a 40% remaining signal was observed after ten successive voltammetric scans (Fig. 2b). This is due to the fact that the zeolite particles are located only on the surface of the MVY-modified PIGE in the first case whereas they are dispersed in the whole volume of the carbon paste matrix (both in the bulk of the electrode and at its surface) in the second one. In this latter case, due to the hydrophilic character of the zeolite particles and the porous character of the composite electrode, the electrolyte solution is likely to diffuse into micrometer-thick regions inside the electrode bulk [35] limiting somewhat

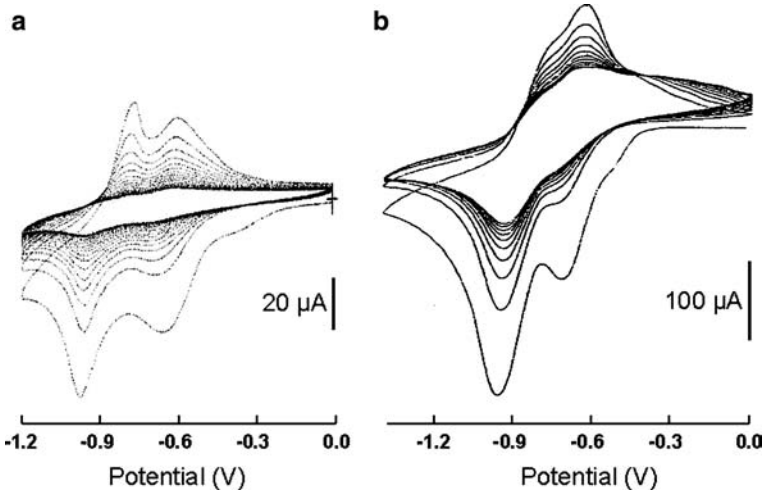

Fig. 2 Multisweep cyclic voltammograms of methylviologen-doped zeolite Y (MVY) supported on PIGE (**a**) or dispersed in a carbon paste electrode (**b**), recorded in 0.1 M $NaNO_3$ directly after immersion of the electrode in the supporting electrolyte solution; **a** first 20 cycles obtained at a scan rate of 200 mV s^{-1} and **b** first 10 cycles obtained at a scan rate of 100 mV s^{-1}

the leaching of MV^{2+} species into the external solution. This is even more dramatic for zeolite-modified carbon paste electrodes containing a lower mineral oil content (up to 80% of the starting CV signal observed when reaching the steady state in multiple successive potential scanning [48]). Such remaining non-negligible signals might be problematic in case of multiple use of the same electrode surface in successive experiments (e.g., voltammetric detection subsequent to open-circuit accumulation [19]) because of the existence of significant "memory effects".

From this point of view, the zeolite-modified PIGE is expected to be more attractive because the zeolite particles involved in the electrochemical processes are only located on the electrode surface in contact to the solution that cannot diffuse into the bulk of the electrode. This is illustrated on Fig. 3 showing the CV response of a zeolite-Y-modified PIGE that has been exposed to a 2×10^{-4} M MV^{2+} solution for 3 min and then transferred to a pure electrolyte medium (i.e., without MV^{2+}) where the voltammetric curves have been recorded in multisweep conditions. The results demonstrated the effective preconcentration of MV^{2+} by ion exchange during the 3-min accumulation step, as illustrated by the well-defined CV signals. The voltammetric peaks were found to drop as fast as cycling potentials continuously as a consequence of the progressive decrease in the MV^{2+} content in the zeolite particles located on the electrode surface. This decrease was even more efficient on exposing the electrode surface to the (stirred) electrolyte solution without scanning potentials because this involved only the MV^{2+} exchange for the electrolyte cations (Eq. 1) and not any leaching-(re)concentration processes arising from the cyclic conversions"$MV^{2+} \rightarrow MV^{\bullet+} \rightarrow MV^{(0)} \rightarrow MV^{\bullet+} \rightarrow MV^{2+} \ldots$" (Eq. 2 abc). This is depicted on Fig. 3 (dashed line) where the CV curve recorded using a zeolite-Y-modified PIGE exposed to a 2×10^{-4} M MV^{2+} medium for 3 min and immersed subsequently to a MV^{2+}-free electrolyte solution for 15 min did not give any measurable current. In comparison, the corresponding zeolite-modified carbon paste electrode still displayed 35% of the initial signal intensity in the same conditions. The chemical regeneration of the zeolite-modified PIGE is faster and more quantitative because of restricted imbibition of the bulk electrode by the external solution in comparison to what occurred in the carbon paste matrix. Note that similar improvements have been also reported when using zeolite-modified screen-printed electrodes [19] or zeolite-modified carbon paste electrodes based on a solid paraffin binder [37].

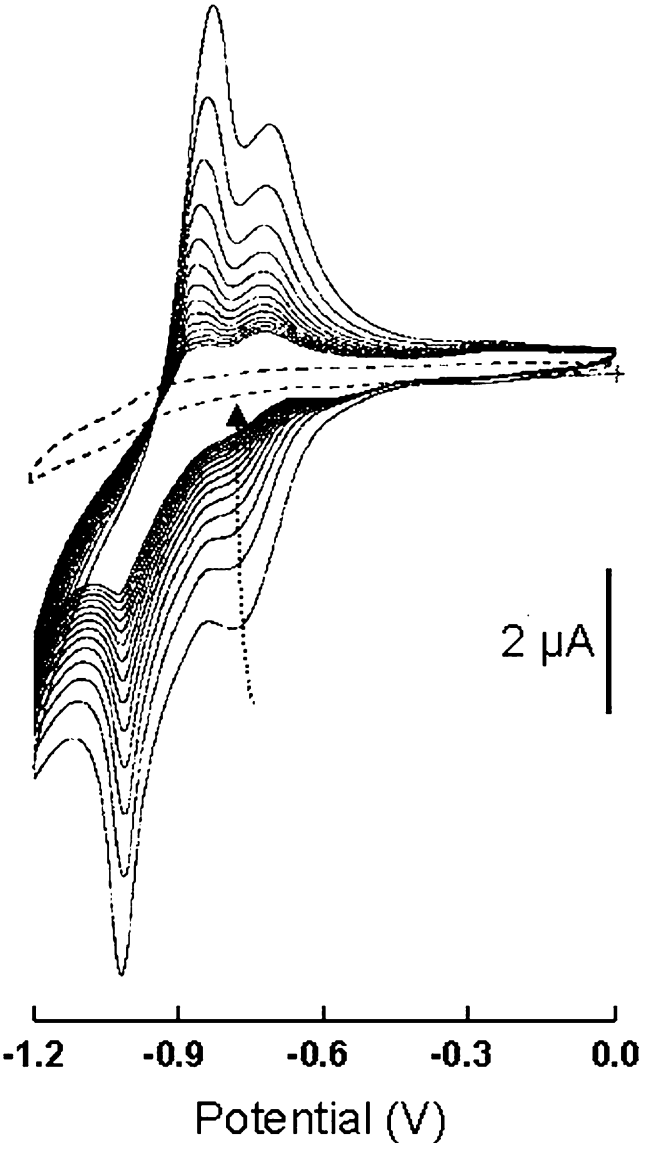

Fig. 3 Multisweep cyclic voltammograms recorded directly after immersion of a NaY-modified PIGE in 0.1 M $NaNO_3$, after 3 min open-circuit accumulation from a 2×10^{-4} M MV^{2+} solution in a separate cell; *solid lines*: first 14 cycles obtained at a scan rate of 50 mV s^{-1}; *dotted line*: CV curve recorded at the same scan rate after 15 min exposure of the electrode to the electrolyte solution

Voltammetric analysis of lead-loaded zeolites after sulfidation

Prior to discussing the electrochemical behavior of (partially) sulfided lead-loaded zeolites, one has to consider the electrochemistry of lead(II) ions exchanged in the zeolite material. Actually, this topic has only been reported in two papers [32, 46]. Ahlers and Talbot [46] have described the electrochemical response of lead(II) at ZMEs prepared by electrophoretic deposition of zeolite particles onto a Pt electrode and covered with a thin Nafion film. In this work, the measurements were carried out only in the cathodic domain (Pb(II)–Pb(0) redox couple), exhibiting CV curves similar to those obtained for lead(II) in solution in agreement with the extrazeolite electron transfer, but characterized by peak currents much higher than on the bare electrode due to the preconcentration by ion exchange. Zhang et al. [32], using a glassy carbon electrode covered by a continuous and thin nanozeolite film, have also found voltammetric

signals located at the same typical values as on the bare electrode and displaying an accumulation capability towards lead(II) cations. Here, the study was extended to the case of lead-loaded zeolite (PbY) particles immobilized on PIGEs, which have been investigated on a wider potential range experienced in CV (i.e., exploring also the anodic region). Some typical results are shown on Fig. 4a representing a CV curve recorded in an unbuffered electrolyte solution, which is characterized by a well-defined cathodic signal located at −0.60 V, corresponding to the reduction of Pb(II) species into metallic $Pb^{(0)}$, and the corresponding anodic stripping peak at −0.42 V on scan reversal, consistent with other studies on ZMEs [32, 46] and with the electrochemistry of lead(II) in solution [58]. Similarly to what was observed for methylviologen-doped zeolite-modified PIGEs (see Section Ion-exchange voltammetry of MV^{2+} above), increasing the exposure time of the electrode to the solution led to a decrease in the peak currents because of the progressive leaching of Pb(II) cations out of the zeolite by ion-exchange for the electrolyte cations. Note that in the conditions applied to fill the zeolite particles with Pb(II) cations, both Pb^{2+} (major) and $Pb_4(OH)_4^{4+}$ (minor) species can be present in the aluminosilicate [41, 42, 45]. When scanning potentials towards the positive direction, Pb(II) species underwent oxidation reactions in the "+1.1 V to +1.4 V" potential range corresponding to the formation of Pb(IV) moieties (electrodeposition of PbO_2) with transient Pb(III) [58, 59]. The PbO_2 deposits were reduced at about +0.75 V on the reverse scan, leading to the generation of OH^- species at the electrode/solution interface [59], which caused the CV peak relative to the reduction of Pb(II) species (actually in the form of $Pb(OH)_2$) on the subsequent voltammetric cycle (dashed line) to shift to a more negative value (at −0.90 V) in comparison to that corresponding to Pb^{2+} reduction (at −0.60 V). This was ascertained by recording a similar CV curve for lead-loaded zeolite Y particles immobilized on PIGE in alkaline medium (pH 12), resulting indeed in a shift of the Pb(II)–Pb(0) redox couple towards more negative values (in Fig. 4b) in comparison to the unbuffered medium (in Fig. 4a). It should be also mentioned that the electrodeposition of PbO_2 by oxidation of $Pb(OH)_2$ at pH 12 occurred at less positive potential (+0.63 V) than in neutral medium, in agreement with the previously reported influence of pH on the deposition–dissolution behavior of PbO_2 on carbon electrodes [59]. Finally, it is noteworthy that PbO_2 arising from the oxidation of the electrochemical oxidation of PbY exhibited a similar voltammetric behavior to that reported for synthetic PbO_2 particles mechanically immobilized on PIGE or dispersed in carbon paste electrodes [60].

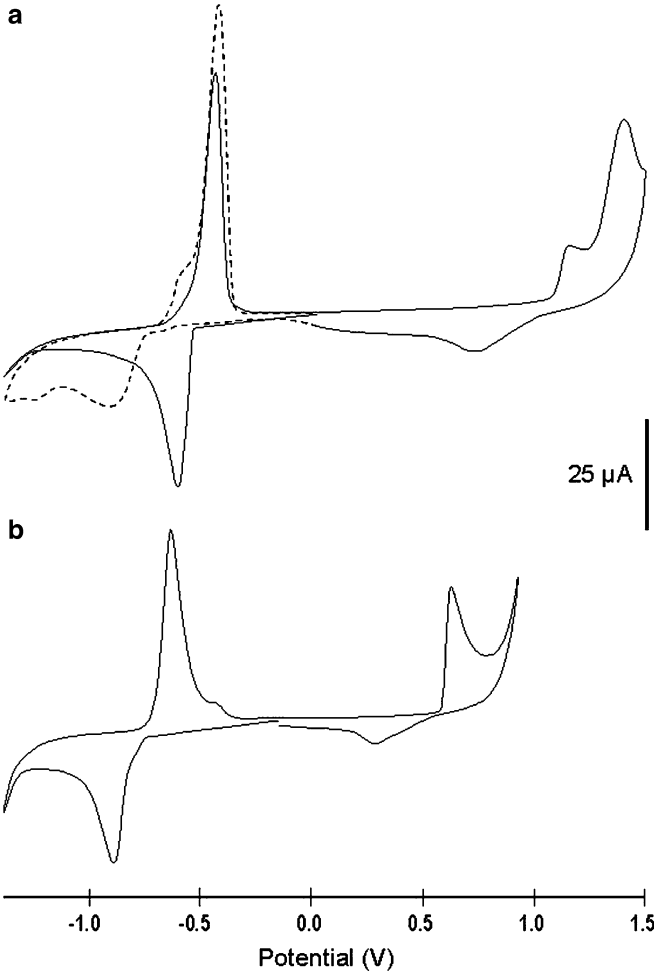

Fig. 4 Cyclic voltammograms of lead(II)-doped zeolite Y (PbY) supported on PIGE recorded in 0.1 M $NaNO_3$ (**a**) or in 0.01 M NaOH + 0.1 M $NaNO_3$ (**b**), directly after immersion of the electrode in the solution, at a scan rate of 5 mV s^{-1}; the *dashed line* depicts the second cycle in case (**a**) in the potential range between 0.0 and −1.5 V

PbY zeolite particles were then sulfided by allowing them to react with sodium sulfide in aqueous suspensions at room temperature. The reaction (Eq. 3) involves the formation of PbS clusters inside the zeolite Y [61, 62] with concomitant charge balance

$$Pb^{2+}_{(Z)} + Na_2S_{(S)} \rightleftharpoons PbS_{(Z)} + 2Na^{+}_{(Z)} \quad (3)$$

maintained by sodium ions. The stoichiometry of reaction (Eq. 3) has been checked by solution-phase analyses of sodium and sulfide moieties, revealing indeed the consumption of two Na^+ cations for one S^{2-} species. It is also expected that the Pb^{2+}/Na^+ exchange would promote the presence of PbS in the cages located on the outermost surface of zeolite particles. The extent of the sulfidation process was first evaluated by XPS measurements by analyzing PbY zeolite particles after reaction with Na_2S at various S/Pb ratios. This is nicely achieved by monitoring the Pb4f lines on the narrow-scanned XPS spectra ($4f_{5/2}$ and $4f_{7/2}$, see Fig. 5a). As shown, increasing the S/Pb ratio resulted in the progressive growing of the Pb $4f_{7/2}$ signal located at a binding energy of 137.6 eV, which can be attributed to PbS [63], associated to a concomitant decrease of the contribution of Pb^{2+} species at the Pb $4f_{7/2}$ binding

energy identified at 140.3 eV. Even more informative is the variation of the relative surface concentration of Si, Al, Na, Pb, and S elements as a function of the sulfidation level. As expected, both the Na and S contributions were found to grow according to Eq. 3 (incorporation of increasing amounts of sulfide by reaction with Pb(II) and ingress of sodium ions to maintain charge balance in the aluminosilicate). More intriguing is the XPS response of the framework Si and Al centers that are not expected to be affected by the sulfidation reaction. In fact, their contribution was found to decrease, especially at high sulfidation levels. As XPS is a surface analysis technique, this decrease suggests the presence of a "shielding" compound that progressively formed on the external surface of the zeolite particles. And this is corroborated by the variation of the Pb line (increasing with the sulfidation level) indicating a concentration of PbS clusters on the external surface of the zeolite particles while the ion-exchanged Pb^{2+} (and $Pb_4(OH)_4^{4+}$) cations were distributed homogeneously in the whole volume of the zeolite particles.

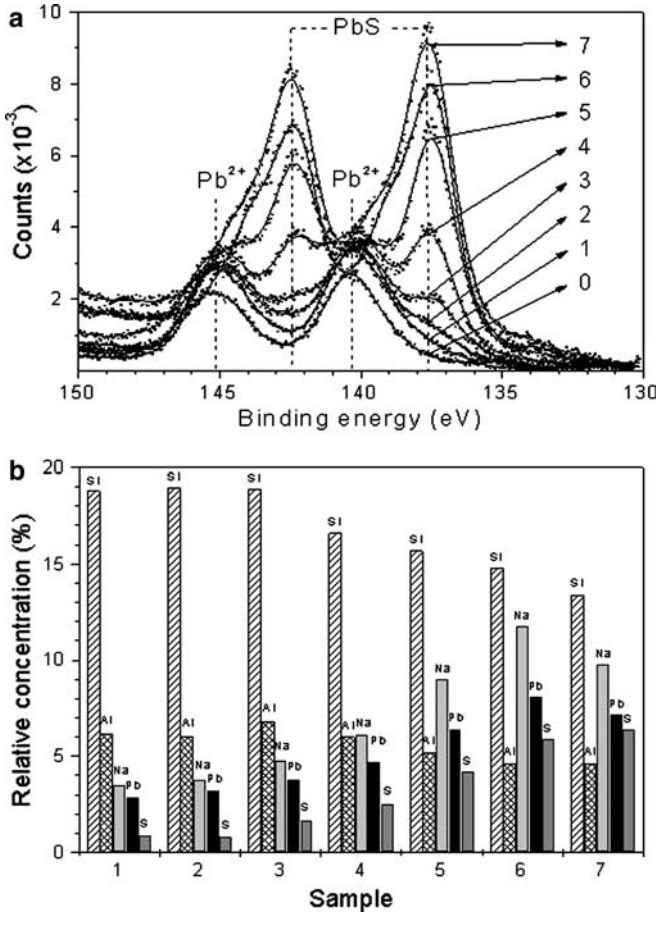

Fig. 5 XPS monitoring of reaction between zeolite PbY and Na_2S at various initial S/Pb ratios: 0.00 (0), 0.05 (1), 0.09 (2), 0.18 (3), 0.45 (4), 0.72 (5), 0.9 (6), and 1.35 (7). **a** XPS spectra of the Pb4f lines; **b** variation of the relative molar surface concentration relative to Si, Al, Na, Pb, and S elements, for samples 1–7

The electrochemical behavior of these sulfided lead-loaded zeolites was studied after mechanical immobilization on PIGE, as a function of the sulfidation level. Typical CV curves obtained with the 5 and 45% sulfided materials are depicted on Fig. 6. The curves "a" and "b" rely on CV experiments performed by exploring the cathodic region on the forward scan and the anodic domain on scan reversal. These curves were very similar to that recorded for the non-sulfided PbY zeolite (curve "a" on Fig. 4) except that peak currents relative to Pb(II) reduction or oxidation were found to decrease when increasing the sulfidation level (compare curves "a" and "b" on Fig. 6), in agreement with the lower Pb^{2+} population in the zeolite. No apparent signal indicative of the presence of PbS was observed. When performing the CV experiments by exploring first the

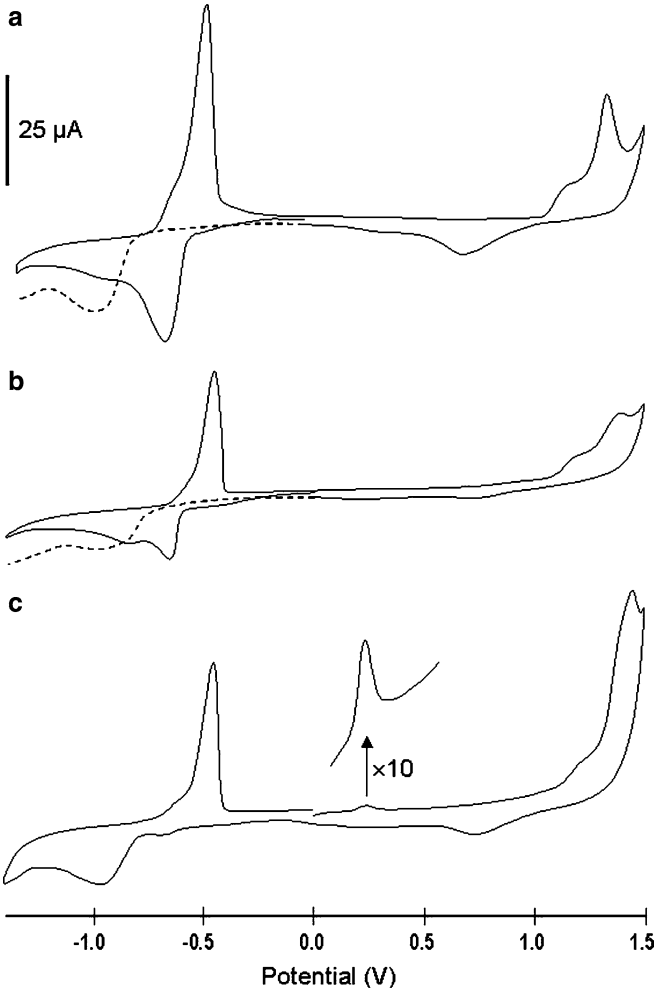

Fig. 6 Cyclic voltammograms of partially sulfided lead(II)-doped zeolite Y supported on PIGE recorded in 0.1 M $NaNO_3$, directly after immersion of the electrode in the solution, at a scan rate of 5 mV s^{-1}; **a** and **b** onward potential scan in the cathodic direction for zeolites with S/Pb ratios of 0.05 (**a**) and 0.45 (**b**); **c** same as **b** but onward scan in the anodic direction; the *dashed lines* depict the beginning of the second cycle in cases (**a**) and (**b**) in the potential range between 0.0 and −1.4 V; the enlargement in curve (**c**) concerns the signal located in the 0.10–0.55 V potential range

anodic region (i.e., forward scan to the positive direction), however, a small additional anodic signal appeared at ca. +0.25 V (see curve "c" on Fig. 6 for the 45% sulfided material). This value is compatible with the anodic dissolution of galena (crystalline PbS) [64] and it will be proven afterward that this anodic peak is really due to the electrochemical oxidation of PbS on the PIGE surface. The very low intensity of this signal in comparison to those of Pb^{2+} species, for a zeolite sample containing approximately the same amount of Pb^{2+} (55%) and PbS (45%) moieties, is clearly due to the high mobility of Pb^{2+} species (that can be exchanged for the electrolyte cation and diffuse out of the zeolite particles to the electrode surface) whereas the PbS clusters are physically trapped in the zeolite cages and/or immobilized on the zeolite particle surface. In spite of their conductive properties, a great part of PbS nanoparticles located inside the zeolite structure are not available for the electron transfer reactions. One can evaluate from the area of the peak located at +0.25 V that no more than 5% of the PbS clusters in/on the zeolite has been involved in the oxidation process, indicating that mostly the "extrazeolite" deposit of PbS particles is responsible for the voltammetric response, the clusters located deeper in the zeolite bulk remaining electrochemically silent. This points out again the difficulty to get intrazeolite electron transfer reactions for electroactive compounds physically immobilized deeply within zeolite particles, as otherwise reported for large electroactive complexes entrapped in zeolite cages [65], the electrochemistry of which being restricted to those species located at the outermost surface of the particle [1].

As the electrochemical behavior of PbS on PIGE has not yet been studied, freshly-prepared PbS particles have been immobilized onto the electrode surface by the abrasive transfer technique [38] and their voltammetric response was investigated by CV in both the anodic and cathodic regions, in conditions as close as possible as those applied for the voltammetric characterization of sulfided lead-loaded zeolites. No attempt was made here to provide a detailed investigation on the influence of the medium composition on the electrochemical behavior of galena; the interested reader being directed to previous reports based on pure galena electrodes [64, 66] or on galena-modified carbon paste electrodes [67, 68]. The main results are summarized on Fig. 7 for both the anodic dissolution (Fig. 7a) and the cathodic reduction (Fig. 7b). PbS was indeed electrochemically oxidized, giving an anodic signal beginning at ca. +0.2 V displaying a shape typical of the electrochemical transformation of a solid phase deposited on the electrode surface. This reaction involves most probably the formation of Pb^{2+} species and elemental sulfur $S^{(0)}$ [64]. On scan reversal, the generated Pb^{2+} species can be reduced in the −0.8 to −1.0 V region, the $Pb^{(0)}$ deposit being stripped off at ca. −0.4 V during the subsequent anodic scan. When performing the forward scan in the cathodic direction, it appeared that PbS can be reduced in the form of a solid phase-typical peak beginning at ca.

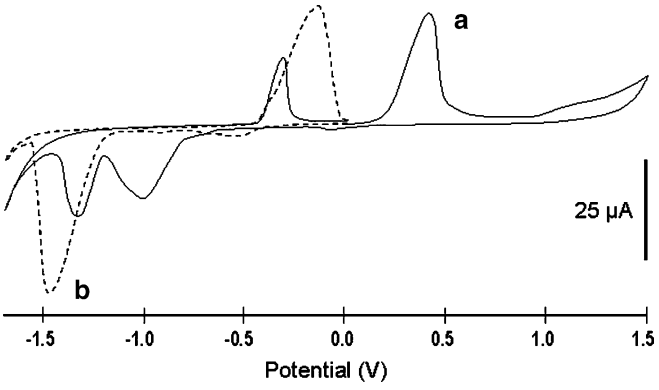

Fig. 7 Cyclic voltammograms of synthetic PbS microparticles immobilized on PIGE recorded in 0.1 M $NaNO_3$ at a scan rate of 5 mV s^{-1}; *plain line* depicts the CV curve obtained by onward potential scan in the anodic direction while the *dashed line* is relative to the onward scan in the cathodic direction

−1.2 V, corresponding to the formation of $Pb^{(0)}$ with concomitant leaching of sulfide moieties. This metallic deposit underwent an anodic stripping transformation on scan reversal. The existence of a PbS reduction peak in the potential region from −1.2 V to −1.5 V explains why it was not possible to detect its presence in the CV curves corresponding to the reduction of partially sulfided lead-loaded zeolites (curves "a" and "b" on Fig. 6), because it was too small and embedded in the tailing of the large Pb^{2+} reduction signal. Anyway, though undetectable, it was really effective as the small peak corresponding to PbS oxidation at +0.25 V was only present when the forward potential scan was made in the anodic direction (curves "c" on Fig. 6) whereas this small peak at +0.25 V was absent when applying the forward potential scan in the cathodic direction, because the small portion of electroactive PbS was reduced in this case and thus no more available for oxidation on scan reversal (curves "b" on Fig. 6). For all these reasons, it was chosen to restrict the electrochemical study of PbS clusters only in the potential region corresponding to its oxidation (0.0 V to +0.6 V). In this case, the response of sulfided lead-loaded zeolite particles immobilized on PIGE was similar to those CV curves recorded with PIGEs modified by the presence of microcrystals of synthetic PbS. The tall peak at +0.25 V is consistent with electron microscopy data [61], indicating that PbS clusters are small and exhibit a homogeneous size distribution.

Figure 8 illustrates how the electrochemical response of the lead-loaded zeolite-modified PIGE is affected by the sulfidation level of the PbY particles. In fact, the PbS clusters became only electrochemically visible at sulfidation levels higher than 5% most probably because two low PbS contents in the zeolite resulted in too small clusters located in the zeolite cages, mostly in the bulk of the particles in agreement with XPS measurements (Fig. 5b). It was therefore necessary to increase the PbS/Pb^{2+} ratio to get more PbS within the zeolite particles

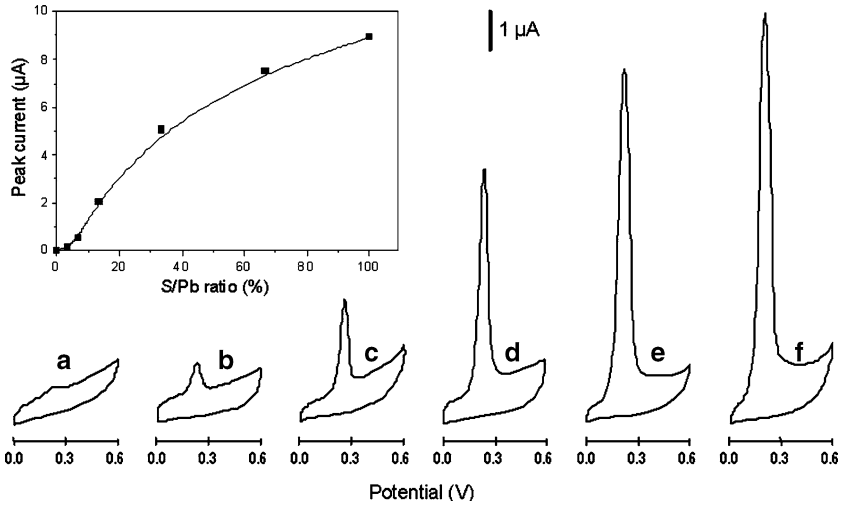

Fig. 8 Influence of the S/Pb ratio of the (partially) sulfided lead-loaded zeolites Y on their voltammetric response in the 0–0.6 V potential range. The data correspond to the following S/Pb ratios: 0.03 (a), 0.07 (b), 0.13 (c), 0.33 (d), 0.67 (e), and 1.0 (f)

with significant enrichment on their shell, which might be detected by anodic oxidation because of direct contact to the electrode surface. At sulfidation levels higher than 5%, the intensity of the voltammetric signals corresponding to PbS oxidation displayed indeed a linear dependence on the S/Pb ratio in the zeolites (i.e., the amount of PbS formed by sulfidation of PbY), as shown on Fig. 8. It is noteworthy, however, that the PbS oxidation signal sampled for the totally sulfided PbY sample (curve "f" in Fig. 8) was still much lower than that corresponding to the redox transformation of Pb^{2+} species ion-exchanged in the non-sulfided PbY zeolite particles, confirming again the preponderance of the extrazeolite electron transfer processes.

Conclusions

This work emphasizes the interest of the abrasive transfer technique to be applied to the voltammetry of microparticles, not only for the study of solid electroactive compounds (as largely exploited otherwise [38, 39, 60]), but also for electrochemical investigations involving non-conductive solid materials (i.e., zeolite particles) containing electroactive moieties in their porous structure. Of particular interest is the possibility to get zeolite particles durably immobilized on the electrode surface without any additive and to apply the resulting device to ion-exchange voltammetry with better performance than, e.g., the zeolite-modified carbon paste electrodes.

The present investigation also describes a novel utility of ZMEs by providing the first example of the electrochemical monitoring of the sulfidation of lead-loaded zeolite Y particles. This has allowed to point out the distinct sulfidation levels and to distinguish between the highly mobile (and exchangeable) Pb^{2+} species giving rise to intense CV signals and the zeolite-supported PbS clusters that were characterized by smaller, yet well-defined, voltammetric peaks.

References

1. Walcarius A (2003) Implication of zeolite chemistry in electrochemical science and applications of zeolite-modified electrodes. In: Auerbach SM, Carrado KA, Dutta PK (eds) Handbook of zeolite science and technology, Chap 14. Marcel Dekker, New York, pp 721–783
2. Rolison DR (1990) Chem Rev 90:867
3. Baker MD, Senaratne C (1994) Electrochemistry with clays and zeolites. In: Lipkowski J, Ross PN (eds) The electrochemistry of novel materials, Chap 7. VCH Publishers Inc., New York, pp 339–380
4. Walcarius A (1996) Electroanalysis 8:971
5. Roué L, Briot E, Bedioui F (1998) Can J Chem 76:1886
6. Walcarius A (1999) Anal Chim Acta 384:1
7. Rolison DR, Bessel CA (2000) Acc Chem Res 33:737
8. Gemborys HA, Shaw BR (1986) J Electroanal Chem 208:95
9. Senaratne C, Baker MD (1992) J Electroanal Chem 332:357
10. Baker MD, Senaratne C (1992) Anal Chem 64:697
11. Ganesan V, Ramaraj R (1998) Langmuir 14:2497
12. Lainé P, Seifert R, Giovanoli R, Calzaferri G (1997) New J Chem 21:453
13. Liu B, Yan F, Kong J, Deng J (1999) Anal Chim Acta 386:31
14. Shaw BR, Creasy KE, Lanczycki CJ, Sargeant JA, Tirhado M (1988) J Electrochem Soc 135:869
15. Wang J, Martinez T (1988) Anal Chim Acta 207:95
16. Creasy KE, Shaw BR (1988) Electrochim Acta 33:551
17. Wang J, Walcarius A (1996) J Electroanal Chem 407:183
18. Walcarius A, Barbaise T, Bessière J (1999) Anal Chim Acta 340:61
19. Walcarius A, Rozanska S, Bessière J, Wang J (1999) Analyst 124:1185
20. Bedioui F, de Boysson E, Devynck J, Balkus KJ Jr (1991) J Electroanal Chem 315:313
21. Bedioui F, Roué L, Devynck J, Balkus KJ Jr (1994) J Electrochem Soc 141:3049
22. Briot E, Bedioui F, Balkus KJ Jr (1998) J Electroanal Chem 454:83
23. Shaw BR, Creasy KE (1988) Anal Chem 60:1241
24. Dryfe RAW, Hayes P, Holmes SM (2001) Analyst 126:733
25. King AJ, Lillie GC, Cheung VWY, Holmes SM, Dryfe RAW (2004) Analyst 129:157
26. Evmiridis NP, Demertzis MA, Vlessidis AG (1991) Fresenius J Anal Chem 340:145
27. Matysik S, Matysik F-M, Mattusch J, Einicke W-D (1998) Electroanalysis 10:98

28. Hamlaoui ML, Reybier K, Marrakchi M, Jaffrezic-Renault N, Martelet C, Kherrat R, Walcarius A (2002) Anal Chim Acta 466:39
29. Bessel CA, Rolison DR (1997) J Phys Chem B 101:1148
30. Bessel CA, Rolison DR (1997) J Am Chem Soc 119:12673
31. Kornic S, Baker M (2002) Chem Commun 16:1700
32. Zhang Y, Chen F, Shan W, Zhuang J, Dong A, Cai W, Tang Y (2003) Microporous Mesoporous Mater 65:277
33. Walcarius A, Ganesan V, Larlus O, Valtchev V (2004) Electroanalysis 16:550
34. Li S,Wang X, Beving D, Chen Z, Yan Y (2004) J Am Chem Soc 126:4122
35. Walcarius A, Lamberts L, Derouane EG (1993) Electrochim Acta 38:2257
36. Wang J, Walcarius A (1996) J Electroanal Chem 404:237
37. Walcarius A, Mariaulle P, Lamberts L (2003) J Solid State Electrochem 7:671
38. Scholz F, Meyer B (1998) Voltammetry of solid microparticles immobilized on electrode surfaces. In: Bard AJ, Rubinstein I (eds) Electroanalytical Chemistry, A Series of Advances. Marcel Dekker Inc., New York, vol 20, pp 1–86
39. Perdicakis M, Aubriet H, Walcarius A (2004) Electroanalysis 16:2042
40. O'Connor JF, Townsend RP (1985) Zeolites 5:158
41. Ronay C, Seff K (1993) Zeolites 13:97
42. Shibata W, Seff K (1997) Zeolites 19:87
43. Maliou E, Malamis M, Sakellarides PO (1992) Water Sci Technol 25:133
44. Petruzzelli D, Pagano M, Tiravanti G, Passino R (1999) Solvent Extr Ion Exch 17:677
45. Walcarius A, Lamdaouar AM, El Kacemi K, Marouf B, Bessière J (2001) Langmuir 17:2258
46. Ahlers CB, Talbot JB (2000) Electrochim Acta 45:3379
47. Pérez-Ruiz T, Martinez-Lozano C, Thomas V (1991) Anal Chim Acta 244:99
48. Walcarius A, Lamberts L, Derouane EG (1995) Electroanalysis 7:120
49. Hui T-W, Baker MD (2001) J Phys Chem B 105:3204
50. Walcarius A, Mariaulle P, Lamberts L (1999) J Electroanal Chem 463:100
51. Walcarius A, Lamberts L, Derouane EG (1993) Electrochim Acta 38:2267
52. Hui T-W, Baker MD (2002) J Phys Chem B 106:827
53. Bird CL, Kuhn, AT (1981) Chem Soc Rev 10:49
54. Calzaferri G, Lanz M, Li JW (1995) Chem Commun 13:1313
55. Sun W, Xue J, Chen J, Mao L, Jin L, Yamamoto K, Tao S, Jin J (1999) Talanta 49:345
56. Hu S (1999) J Electroanal Chem 463:253
57. Suib SL, Morse BE (1989) Langmuir 5:1340
58. Kuhn AT (ed) (1979) The electrochemistry of lead. Academic, London
59. Velayutham D, Noel M (1991) Electrochim Acta 36:2031
60. Zakharchuk N, Meyer S, Lange B, Scholz F (2000) Croat Chim Acta 73:667
61. Flores-Acosta M, Sotelo-Lerma M, Arizpe-Chavez H, Castillon-Barraza FF, Ramirez-Bon R (2003) Solid State Commun 128:407
62. Chen W, Wang Z, Lin Z, Qian J, Lin L (1996) Appl Phys Lett 68:1990
63. Wagner CD, Naumkin AV, Kraust-Vass A, Allison JW, Powell CJ, Rumble JR (2003) NIST Standard Reference Database 20, NIST XPS Database Version 3.4 (Web Version)
64. Paul RL, Nicol MJ, Diggle JW, Saunders AP (1978) Electrochim Acta 23:625
65. Senaratne C, Zhang J, Baker MD, Bessel CA, Rolison DR (1996) J Phys Chem 100:5849
66. Nicol MJ, Paul RL, Diggle JW (1978) Electrochim Acta 23:635
67. Lamache M, Bauer D, Pegouret J (1981) Electrochim Acta 26:1845
68. Ahlberg E, Asbjörnsson J (1993) Hydrometallurgy 34:171